

Ultrasound-controlled cell aggregation in a multi-well chip†

Bruno Vanherberghen,[‡] Otto Manneberg,[§] Athanasia Christakou,[‡] Thomas Frisk,[‡] Mathias Ohlin,[‡] Hans M. Hertz,[‡] Björn Önfelt^{*ab} and Martin Wiklund^{*a}

Received 30th March 2010, Accepted 30th July 2010

DOI: 10.1039/c004707d

We demonstrate a microplate platform for parallelized manipulation of particles or cells by frequency-modulated ultrasound. The device, consisting of a silicon-glass microchip and a single ultrasonic transducer, enables aggregation, positioning and high-resolution microscopy of cells distributed in an array of 100 microwells centered on the microchip. We characterize the system in terms of temperature control, aggregation and positioning efficiency, and cell viability. We use time-lapse imaging to show that cells continuously exposed to ultrasound are able to divide and remain viable for at least 12 hours inside the device. Thus, the device can be used to induce and maintain aggregation in a parallelized fashion, facilitating long-term microscopy studies of, *e.g.*, cell–cell interactions.

Introduction

Microtiter plates are today widely used as a standard tool for diagnostic and analytical purposes.¹ Recent research needs demand microplates with an increased number of wells and/or decreased well dimensions. Examples include screening and culturing of cells where each well is loaded with single² or few³ cells. Although it is possible to both inject² and eject⁴ one cell per well in a controlled manner, there is no simple method available for controlled aggregation and/or positioning of cells in a pre-determined location in each well for the study of, *e.g.*, cell–cell interactions. In this article, we use frequency-modulated ultrasound for parallel aggregation and positioning of cells in a 100-well microplate designed for the studies of individual cells or intercellular interactions involving low numbers of cells.

Plates of standard formats (96–96 000 wells) aimed for *in vitro* cell assays are primarily used for studying cell population responses to varied experimental conditions, such as concentration of soluble factors or cell type. On the other hand, other applications require techniques for studying the distribution within a cell population instead of measuring average values. For this purpose, flow cytometers or fluorescence-activated cell sorting (FACS) machines are routinely used, offering high-throughput quantification of a set of cellular parameters. A limitation of flow cytometry technology, however, is the lack of a time-dependent monitoring function for individual cells. This can instead be achieved with live cell imaging microscopy, albeit with limited throughput. In a recent study, flow cytometry

and microscopy were combined with a multi-well platform for time-dependent screening of a population of isolated single cells.⁵ Still, there is no simple method available for controlling/inducing cell–cell interactions in a highly parallel manner.

Ultrasonic manipulation of particles or cells in microfluidic systems is an expanding research field and has been used for, *e.g.*, continuous separation, concentration, trapping and sensing applications.^{6–8} The technology has also been applied for particle aggregation and positioning in standard 96-well plates, but until now only demonstrated in one single well.⁹ Parallelization of the technology has previously been demonstrated in closed single-volume microdevices by the use of two different approaches, either by parallelization of channel-integrated ultrasonic transducers,^{10,11} or by employing multi-wavelength (mm scale) fluid chambers for two-dimensional (2D) arraying/patterning of suspended particles.^{12–17} However, in these systems crosstalk between nearby trapping sites in the array is difficult to avoid. Therefore, such devices are less suitable for the studies of individual cell–cell interactions.

We have recently introduced the concept of ultrasonic caging of cells in three dimensions in a closed (pump-driven) microfluidic chip.¹⁸ An ultrasonic cage is a geometric feature of a microchannel segment designed to host three orthogonal half-wave acoustic resonances. Incident cells are trapped three-dimensionally in the center of the cage when the chip is actuated at two¹⁸ or more¹⁹ ultrasonic frequencies. In the present article, we apply the cage concept to an open (flow-free) multi-well plate for simultaneous aggregation and positioning of cells in 100 parallel cages. The microchip is devised for real-time confocal-fluorescence-microscopic characterization of cellular interactions in a parallelized fashion.³ Frequency-modulated ultrasonic actuation¹⁹ is employed to achieve homogenous trapping in all 100 wells, and the experimental performance is compared with theoretical simulations. Furthermore, the biocompatibility of the device is investigated by studying the cell viability during more than 12 hours of continuous ultrasonic caging of cells. This is a significant extension in time compared to previous studies in ultrasound-driven microsystems, which were limited to approximately 1 hour of biocompatible manipulation of mammalian cells.²⁰

^aDepartment of Applied Physics, Royal Institute of Technology, AlbaNova University Center, SE-106 91 Stockholm, Sweden. E-mail: martin.wiklund@biox.kth.se; bjorn.onfelt@ki.se

^bDepartment of Microbiology, Tumor and Cell Biology, Karolinska Institutet, SE-171 77 Stockholm, Sweden

† Electronic supplementary information (ESI) available: Videos demonstrating the positioning effect of single frequencies and frequency modulation on beads and cells, and cellular division under continuous ultrasound exposure. See DOI: 10.1039/c004707d

‡ Contributed equally.

§ Current address: Biomedical Imaging Laboratory, Department of Environmental Health, Harvard School of Public Health, 665 Huntington Avenue, Boston, MA 02115, USA.

Methods

Device

The microchip, illustrated schematically in Fig. 1, consists of a $22 \times 22 \times 0.3$ mm³ silicon layer anodically bonded to a $22 \times 22 \times 0.175$ mm³ glass layer. In the center of the silicon layer, a 10×10 array of $0.3 \times 0.3 \times 0.3$ mm³ wells (with 10 μ m corner radii in the horizontal plane and separated by 100 μ m thick walls, *cf.* Fig. 2 and 3 and ESI video S1†) was fabricated using standard dry-etching technology. Apart from heat oxidation, no other surface modification or coating was employed. The chip is actuated by an ultrasonic wedge transducer²¹ (45° angle, 20 \times 7 mm² base area) assembled with a water-soluble conductive adhesive gel ('Tensive', Parker Laboratories, USA), with its back baseline aligned with one of the chip edges (*cf.* Fig. 1). A detailed description of the wedge-transducer design is found in ref. 21. In brief, the wedge transducer generates Lamb-type oscillations of the silicon-glass chip, which are coupled to pressure waves in the fluid-filled wells. The dimension of the wells corresponds to roughly half the acoustic wavelength in water, in order to generate a single-pressure-node standing wave in each well. The transducer was driven at up to 10 V_{pp} (volts peak-to-peak), either at selected single frequencies within the interval 2.55–2.65 MHz, or with linear frequency sweeps between 2.55 and 2.65 MHz at a rate of 1 kHz (*cf.* Fig. 2). A small gasket of polydimethylsiloxane (PDMS) was placed on the chip surrounding the wells as a receptacle and cell culture media (approx. 200–300 μ l) were placed within. A high-concentration sample of 5 μ m polyamide beads ($>10^8$ beads ml⁻¹), or 50 μ l of dye-labeled cells (30 000 cells ml⁻¹) were added and left to sediment by gravity with the ultrasonic actuation turned on. The temperature was monitored with two type-T thermocouple microprobes (IT-21, Physitemp Instruments, Clifton, NJ, USA) either attached by the 'Tensive' conductive gel to different positions on the upper surface of the chip, or placed directly in the fluid sample inside the PDMS gasket. The system was sealed by adding a glass coverslip on top of the PDMS gasket (cf. Fig. 1) and placed on a heatable microscope stage inside an environmental chamber (Pecon GmbH, Incubator S-M, Germany) kept at 37 °C and 5% CO₂ concentration. Fluorescence images were acquired with a Zeiss LSM 5 Pascal confocal

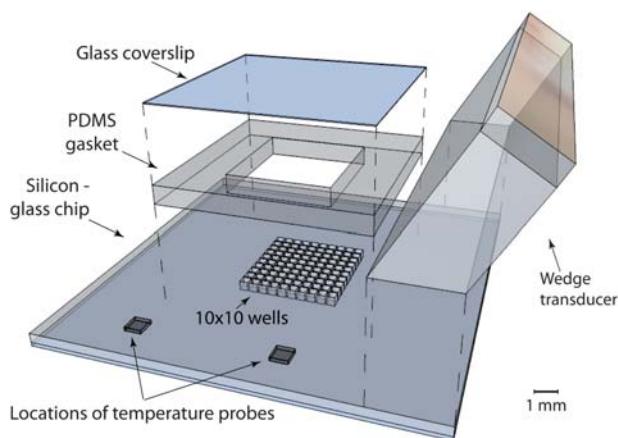


Fig. 1 Schematic drawing of the different parts of the device. The device is assembled by moving the PDMS gasket, the coverslip and the transducer down onto the chip.

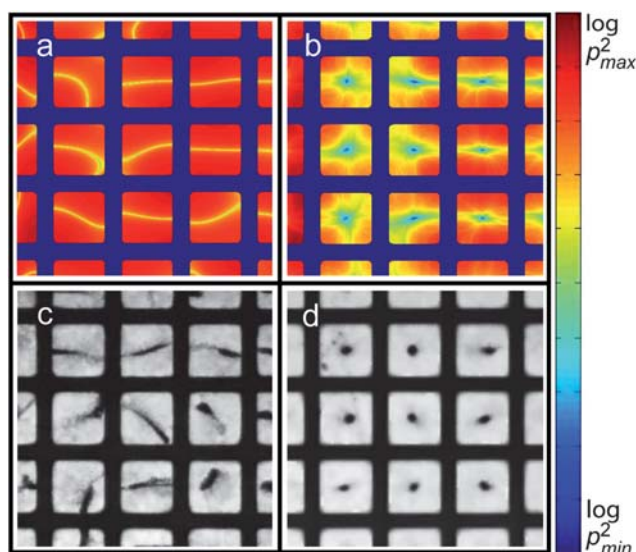


Fig. 2 Simulation of the time-averaged pressure squared (p^2) for single frequency actuation at 2.60 MHz (a) and for the average of 50 single frequencies between 2.55 and 2.65 MHz (b). Both plots are normalized individually and shown in logarithmic scale. The color bar goes from blue (minimum value) over yellow to red (maximum value). Thus, predicted trapping locations (*i.e.*, the minima of p^2) are indicated in yellow (in a) and in dark blue (in b). Experimental confirmation of simulations using 5 μ m beads at single frequency (c) and with frequency modulation (d) using the same intervals as (a) and (b). Scale bar is indicated by the wells (0.3 \times 0.3 mm each).

microscope equipped with a $10\times/0.3$ NA objective. The pinhole was opened to capture maximum fluorescence and images were acquired by sequential tile scanning over all 100 wells. For cell viability studies samples were imaged every 3 hours for at least 12 hours while images were acquired every 4 minutes for up to 12 hours to capture cell division. The resulting image mosaics were 4×4 tiles scans of 1024×1024 pixels yielding final images of 4096×4096 pixels, corresponding to a sub- μ m per pixel resolution, *cf.* ESI video S1†.

Cell culture and labeling

The non-adherent human B cell line 721.221/HLA-Cw6 was maintained in RPMI-1640 media supplemented with 10% FCS, 2 mM L-glutamine, $1\times$ non-essential amino acids, 1 mM sodium pyruvate, 50 U ml⁻¹ penicillin–streptomycin, and 50 μ M β -mercaptoethanol at 37 °C, 5% CO₂. 2×10^6 Cells were labeled with 1 μ M ml⁻¹ calcein-AM (Invitrogen) at 37 °C, 5% CO₂ for 10 minutes. After staining, cells were washed two times in RPMI-1640.

Image analysis

Acquired tile scans were reconstructed using in-house developed MATLAB routines. Cell viability was determined based on the presence of calcein fluorescence and a visibly intact cell membrane. Cells that did not meet these criteria were scored as dead. To create image overlays of the cell distribution with the microchip in the absence or presence of ultrasound (*cf.* Fig. 4c and d), individual wells were cropped and converted into a stack and then overlaid using a z -projection algorithm (ImageJ).

Results and discussion

Frequency modulation: Simulation and experimental verification

To optimize the design of the multi-well structure, acoustic resonances in the silicon layer (including the fluid-filled wells) were modeled in 2D by the finite element method (FEM) software Comsol Multiphysics. The output of the FEM simulations is the displacement field in the solid structure (silicon) and the pressure field p in the fluid (*i.e.*, the wells). The time-averaged acoustic radiation force F on a particle suspended in a fluid can be calculated as the gradient of a force potential U , which is a function of the acoustic pressure amplitude p :^{22,23}

$$U = \frac{V_p \beta_f}{4} \left[f_1 p^2 - \frac{3}{2k^2} f_2 (\nabla p)^2 \right] \quad (1)$$

where

$$F = -\nabla U, \quad (2)$$

$$f_1 = 1 - \frac{\beta_p}{\beta_f} \quad \text{and} \quad f_2 = 2 \frac{(\rho_p - \rho_f)}{2\rho_p + \rho_f} \quad (3)$$

Here, V_p is the volume of the particle, $\beta = 1/(\rho c^2)$ is the compressibility (defined by the density, ρ , and the sound speed, c), $k = \omega/c$ is the wave number, and f_1 and f_2 are the acoustic contrast factors defined by the compressibility β and the density ρ . The index “ f ” denotes “fluid” and the index “ p ” denotes “particle”. Eqn (1)–(3) are valid for a single particle or cell, where eqn (2) is referred to as the primary acoustic radiation force. The secondary (particle–particle interaction) contribution to the acoustic radiation force is a small effect²⁴ that is expected to have no influence for the small cell numbers studied in this work, and is therefore not considered in our simulations.

Fig. 2a and b show the results of FEM simulations investigating the effects of single frequency actuation at 2.60 MHz (Fig. 2a), and frequency modulation around a 2.60 MHz center frequency with a bandwidth of 100 kHz, using linear sweeps at a rate of 1 kHz (Fig. 2b). The frequency modulation is here modeled by averaging the fields from 50 evenly spaced single frequencies between 2.55 MHz and 2.65 MHz, in steps of 2 kHz. In Fig. 2, we have plotted a 3×3 well area, since a full 10×10 well plot would not reveal the finer details. However, the 3×3 well plot is representative of the full 10×10 well area. The full 10×10 well experimental performance is shown in the ESI movie S1†. In Fig. 2a and b, the plotted parameter is the normalized square of the modeled pressure field p^2 . The locations of the minima of p^2 are approximately the same as the minima of the force potential U (eqn (1)).¶ This approximation can be made since $f_1 \gg f_2$ for a polyamide bead or cell in a water-based medium (*cf.* eqn (3)), and $(\nabla p)^2$ is small in proximity to a pressure node. In other words, the first term of eqn (1), which is proportional to p^2 , strongly dominates over the second term close to a trapping location. Thus, suspended particles or cells are

expected to be driven to positions of minimum pressure squared, *i.e.*, the yellow areas in Fig. 2a, and the blue areas in Fig. 2b. The reason for the apparent difference in range of p^2 between Fig. 2a and b is due to the hardly resolved fine structure (small blue spots) within the yellow nodal lines in Fig. 2a. This is due to simulation artifacts, enhanced by the logarithmic scale.

In Fig. 2c and d, the simulations are verified experimentally by imaging the pattern of trapped 5 μm beads after a few minutes of ultrasound actuation at 10 V_{pp} , using the same frequencies as modeled in Fig. 2a and b. Typically, for single-frequency actuation (Fig. 2c) the beads are trapped in elongated, curved patterns spread across the full widths of the wells. The aggregates have more or less arbitrary orientations with their center of mass positioned almost randomly, sometimes close to the well centers, and sometimes close to the well walls. Furthermore, the trapping efficiency (*i.e.* the magnitude of the forces) also differs from well to well which leads to a variation in size and density of the final particle agglomerate, as well as the time to reach a near-static particle distribution (the latter typically varied from a few seconds up to a minute). When manually changing the actuation frequency in steps of 10 kHz within the examined range (2.55–2.65 MHz), a similar modeled pressure field as in Fig. 2a and a similar experimental pattern of trapped beads as in Fig. 2c are found. In individual wells, the orientation of modeled minimum pressure squared and the shape and position of the bead agglomerate vary with frequency, but the overall pattern is similar. This is experimentally visualized in the ESI movie S1†, where we perform manual frequency modulation by a very slow sweep from 2.55 to 2.65 MHz in steps of 10 kHz (approx. 1 minute actuation per frequency). Thus, the result of the fast (1 kHz rate) frequency modulation experiment in Fig. 2d is an averaging effect of all the single-frequencies. When the modulation is faster than the time-scale of the particle motion,²⁵ the particles are confined in small near-circular spots centered in all 100 wells. This is also predicted in the simulation shown in Fig. 2b, where the average of all 50 single-frequency pressure fields form a small trapping spot close to the center of each well. This corresponds approximately to the position of the intersection of 50 curves of minimum pressure squared (*cf.* yellow curves in Fig. 2a).

Temperature control

Application of ultrasound typically results in an increase in temperature due to electromechanical losses in the transducer and acoustic absorption in lossy materials such as the glue layers. To allow long-term manipulation of cells within our device (>hours), it is crucial to control and maintain a stable temperature. We have previously shown that it is possible to regulate the temperature in the fluid channel of a closed, flow-through chip, by first measuring the temperature increase due to the ultrasound and then calibrating the external heating system to account for this.²⁶ We applied a similar strategy in this work. First, we measured the dependence of temperature on actuation frequency using a probe attached to the upper surface of the chip next to the transducer (Fig. 3a). The maximum temperature increase occurred for the frequencies closest to the optimal chip resonance around 2.60 MHz, also corresponding to the optimal manipulation effect. Next, we measured the temperature dependence on

¶ We noticed that p^2 -plots in logarithmic scale display the predicted trapping locations more distinctly than U -plots, thus more resembling the experimental images. We believe this could be due to simulation artifacts originating from the calculated ∇p -terms in U or F . However, there is no visible difference in locations of the minima between p^2 -plots and U -plots, only better contrast in the p^2 -plots.

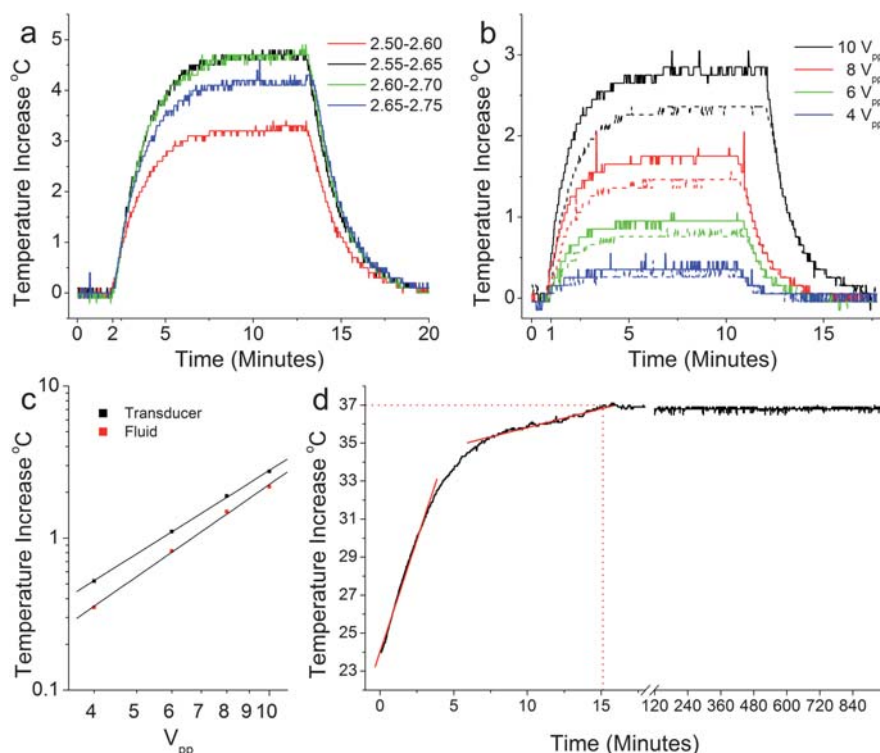


Fig. 3 Temperature control. (a) The temperature dependency on actuation frequency was measured using various frequency modulation schemes at 10 V_{pp}. Optimal performance was found for 2.55–2.65 MHz (black curve). Temperature was measured adjacent to the transducer. (b) Temperature dependence on the voltage applied over the transducer was monitored adjacent to the transducer (solid lines) and within the fluid in the microwells (dotted lines). (c) The temperature increase proportional to the voltage squared (exponents are 1.82 ($R^2 = 0.9998$) and 2.01 ($R^2 = 0.9984$) for the transducer and fluid respectively), data extracted from (c). (d) Temperature calibration and maintenance at 37 °C using internal ultrasound heating and external chamber/stage heating simultaneously. Red lines show the approximate rates of the faster ultrasonic and slower chamber/stage heating. Dotted red lines indicate the target temperature as well as the time required to reach it.

the voltage applied over the transducer (Fig. 3b). Here, one probe was attached to the upper surface of the chip next to the transducer, and one immersed in the sample fluid in the wells (*i.e.*, inside the sealed fluid-filled PDMS receptacle, *cf.* Fig. 1),

thus monitoring the transducer and well temperatures, respectively. As seen in the diagram, the temperature increase is proportional to the voltage squared, with approx. 6 minutes rise time until the temperature is stabilized for the maximum voltage

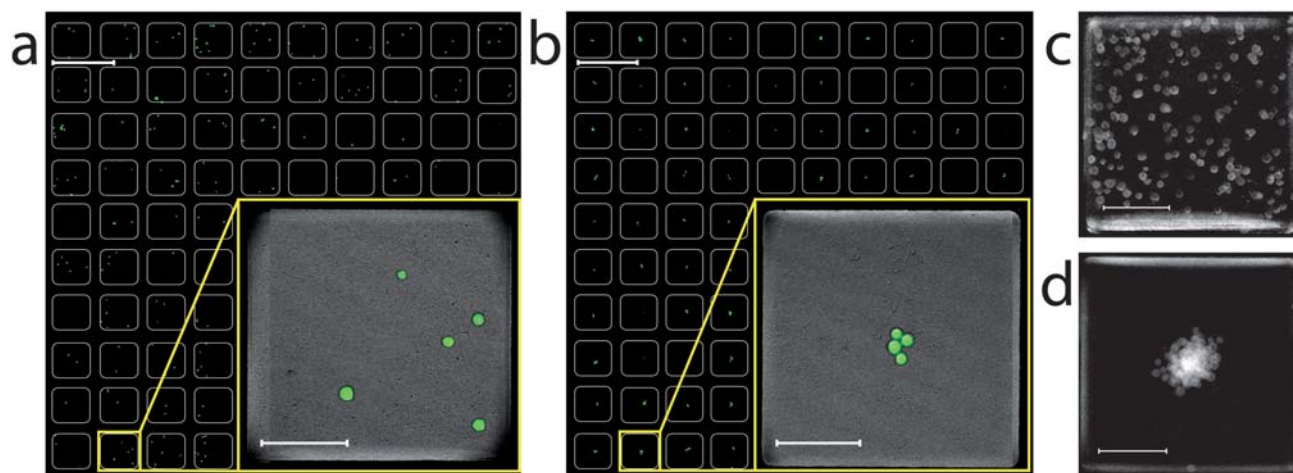


Fig. 4 Tile scan of the device showing the 10 × 10 well structure seeded with calcein-labeled human B cells in the absence (a) or presence (b) of ultrasound. Insets in (a) and (b) show enlarged images of a single well for each condition. The distribution of 195 cells from individual wells was superimposed in a single well in the absence (c) or presence (d) of ultrasound. Scale bars in full image in (a) and (b) represent 500 μm. The scale bars in the inset in (a) and (b) as well as (c) and (d) represent 100 μm.

used ($10 V_{pp}$, Fig. 3c). The difference between the transducer and fluid temperature increases slightly with voltage, and is 0.47 ± 0.13 °C at $10 V_{pp}$. The absolute temperature increase in the fluid varied slightly between different experiments and was 3.26 ± 1.08 °C at $10 V_{pp}$ actuation voltage (*cf.* Fig. 3a and b). This range depended primarily on the fluid volume within the PDMS receptacle (larger fluid volume results in smaller temperature increase, but also weaker radiation forces), but also on the specific transducer used and its position/orientation on the chip. We also noted a temperature gradient over the chip surface (from the transducer to the opposite corner of the chip, *cf.* Fig. 1) of about 1 °C (data not shown), corresponding to 0.08 °C mm^{-1} (*i.e.*, 12 mm between the probes). This gradient is in agreement with previous results in a closed microfluidic chip.²⁶

Finally, we demonstrate how the results in Fig. 3a and b can be used for maintaining the optimal temperature 37 °C during device operation (Fig. 3d). Here, we use the increase in temperature from the ultrasound as calibration data for the environmental chamber and temperature controlled microscope stage and chip holder. Note the two different slopes of the transient part of the curve, corresponding to the faster ultrasonic heating (2.0 °C min^{-1}) and slower chamber/stage heating (0.2 °C min^{-1}). Overall, it takes about 15–20 min to stabilize the temperature of the device. When this transient phase has passed, the temperature can be kept stable over long periods (with a standard deviation of 0.02 °C over 15 hours, *cf.* Fig. 3d). However, due to the measured temperature gradient over the chip surface (0.08 °C mm^{-1}), we may have a 0.3 °C difference between the first and the last well row (estimated as the worst case).

Positioning and aggregation of cells

The cell positioning and aggregation performance of the device are demonstrated in Fig. 4. Here, we used a calcein-labeled non-adherent human B cell line and confocal fluorescence imaging. Fig. 4a and b show the resulting cell distributions without and with ultrasonic actuation, respectively, after seeding the chip with a concentration of cells to obtain approximately 1–5 cells per well. The ultrasound was turned on and the system was

temperature-stabilized prior to seeding the cells in the PDMS receptacle. As exemplified in the insets in Fig. 4a and b, sub-cellular resolution is obtained when zooming in on a single well (see also the ESI movie S1†). The trapping efficiency can be quantified by measuring the positioning performance and the aggregation performance. To indicate the positioning performance, the full 10×10 well images in Fig. 4a and b were cut into individual wells and arranged in a stack using ImageJ. The *z*-projections of these stacks are shown in Fig. 4c and d (ultrasound off and on, respectively), displaying the superimposed spatial distribution of the cells in all wells. Since the total cell number was higher in Fig. 4a than in 4b, we superimposed the same number of cells for a consistent presentation of the data. In contrast to the random distribution of cells covering the full well area in the absence of ultrasound (Fig. 4c), ultrasound exposure (Fig. 4d) demonstrates a clearly confined distribution of cells in the middle of the wells. More specifically, 90% of the cells in Fig. 4d were positioned in an area corresponding to 4% of the full well area (within approx. 60×60 μm^2), and >99% of all cells were positioned in an area corresponding to 9% of the full well area (within approx. 90×90 μm^2). Finally, the aggregation performance was measured by counting the number of cells aggregated in single clusters (*i.e.* with visible cell–cell contact). Here we only consider the wells containing more than one cell. From five different experiments ($n = 867$), we obtained $96.7 \pm 4.2\%$ cells in aggregates.

Effect of ultrasound exposure on cell viability

Previous studies in microsystems have shown that mammalian cells remain viable for at least 1 hour under constant ultrasound exposure at similar acoustic powers as used here (*i.e.*, corresponding to approx. 0.5–1 MPa acoustic pressure amplitudes).²⁰ Our multi-well system has an advantage to microfluidic devices as trapped cells cannot be disturbed or flushed out by air bubbles or instabilities in the fluid, which is often the limiting factor when aiming for experiments exceeding one hour. Furthermore, a non-surface-coated multi-well chip is biocompatible for non-adherent cells.³ In this study, we determined whether continuous

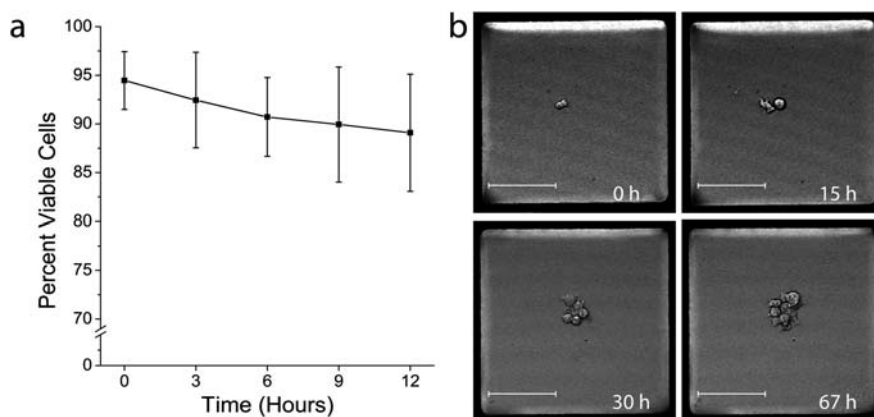


Fig. 5 Viability study. (a) Calcein-labeled human B cells were seeded in the device and exposed to continuous ultrasound for a period of at least 12 hours. Images were scanned every 3 hours and viable cells were scored as described in the Methods section. In total, 4482 cells were counted. The results are compiled from three independent experiments and error bars are standard deviations of the mean. (b) A representative sequence of images showing a single trapped cell proliferating into a cluster of several cells while exposed to 67 hours of continuous ultrasound. The scale bar is 100 μm .

ultrasound exposure affected cellular viability within our system over a longer time period than investigated in ref. 20. Subjecting non-adherent human B cells trapped within the 100 wells to continuous ultrasound exposure (10 V_{pp}, frequency modulation 2.55–2.65 MHz@1 kHz sweep rate) for 12 hours demonstrated that cellular viability was not compromised during this period (Fig. 5a). Ultrasonic exposures for up to 72 hours showed that cells were able to divide several times. For example, a single cell trapped within the center of a well could divide several times to yield a clonal population while permanently exposed to ultrasound (*cf.* Fig. 4b and ESI video S2†). Furthermore, by increasing the frequency of image acquisition, cellular division could also be captured (ESI movie S2†). Together, these data indicate that the ultrasonic forces generated are strong enough to retain the cells in the center of the wells over long time periods without negatively affecting their viability.

Summary and conclusions

We have shown that ultrasonic particle manipulation can be applied to an open multi-well microplate for parallelized aggregation of cells at predetermined locations. This was here demonstrated in a 100-well microplate designed for the studies of individual immune cell interactions by high-resolution optical microscopy. In contrast to single-well, single-frequency operation,¹⁸ the parallelization was accomplished by a frequency modulation scheme, which made it possible to aggregate and center cells in all 100 wells and keep them stably positioned over long time periods. Furthermore, in contrast to previous studies of parallelization of the technology,^{10–17} our device ensures identical but physically separated biochemical environments. For example, it is possible to use the ultrasound for aggregating the cells and then turn it off without the risk of losing track of the individual aggregates.

Furthermore, our results show that >99% of the cells remain positioned and aggregated over more than 12 hours within an area corresponding to the field of view of a 100× objective with high NA for standard optical microscopy (*i.e.*, 90 × 90 μm field of view for the 100×/1.3 NA oil immersion objective used in ref. 18). This makes it possible to program the microscope stage and camera to acquire one such high-resolution image per well, corresponding to a factor 20 in decreased scanning time of the full plate. Additionally, this allows high-resolution imaging of up to 100 individual cells in a parallelized fashion. An alternative to ultrasound-based aggregation of cells is to use smaller well dimensions and coincidence-based interaction due to the mobility of effector cells. While ultrasound aggregates the cells within seconds, such coincidence-based interactions (without ultrasound) result in a spread in starting time of several hours or even days in similar sized wells.³ Smaller wells (*i.e.*, a few cell diameters wide) can decrease this time, but our relatively large well dimension of 0.3 × 0.3 mm is more suitable for proliferation studies without the risk of overflowing the wells with cells.

Finally, the described device is both robust and gentle. Quantification of cellular viability during 12 hours of continuous ultrasound exposure demonstrated no significant increase in cell death. However, it is possible that ultrasound exposure affects other processes, such as the rate of cellular proliferation. This remains to be determined. It should be noted, however, that in

the viability study performed here, the cells were exposed to continuous ultrasound over the full time period. An alternative of device operation is to use the ultrasound only initially for inducing the cell–cell contact and then turn it off. In the future, we plan to use the device for coordinating the starting time of interaction between individual immune cells in a highly parallel manner, in order to study the dynamics of immune synapses. Such interactions typically occur over time scales ranging from minutes up to several hours.³

Acknowledgements

Financial support is gratefully acknowledged from the Swedish Research Council, the Göran Gustavsson Foundation, the Swedish Foundation for Strategic Research, the Åke Wiberg foundation, and the Magnus Bergvall foundation.

References

- 1 Y. Tanaka, K. Sato, T. Shimizu, M. Yamato, T. Okano and T. Kitamori, *Biosens. Bioelectron.*, 2007, **23**, 449–458.
- 2 Y. Tokimitsu, H. Kishi, S. Kondo, R. Honda, K. Tajiri, K. Motoki, T. Ozawa, S. Kadowaki, T. Obata, S. Fujiki, C. Tateno, H. Takaishi, K. Chayama, K. Yoshizato, E. Tamiya, T. Sugiyama and A. Muraguchi, *Cytometry, Part A*, 2007, **71**, 1003–1010.
- 3 K. Guldevall and B. Önfelt, unpublished work.
- 4 J. R. Kovac and J. Voldman, *Anal. Chem.*, 2007, **79**, 9321–9330.
- 5 S. Lindstrom, R. Larsson and H. A. Svahn, *Electrophoresis*, 2008, **29**, 1219–1227.
- 6 A. Lenshof and T. Laurell, *Chem. Soc. Rev.*, 2010, **39**, 1203–1217.
- 7 M. Wiklund and H. M. Hertz, *Lab Chip*, 2006, **6**, 1279–1292.
- 8 L. A. Kuznetsova and W. T. Coakley, *Biosens. Bioelectron.*, 2007, **22**, 1567–1577.
- 9 M. Wiklund, J. Toivonen, M. Tirri, P. Hanninen and H. M. Hertz, *J. Appl. Phys.*, 2004, **96**, 1242–1248.
- 10 T. Lilliehorn, U. Simu, M. Nilsson, M. Almqvist, T. Stepinski, T. Laurell, J. Nilsson and S. Johansson, *Ultrasonics*, 2005, **43**, 293–303.
- 11 T. Lilliehorn, M. Nilsson, U. Simu, S. Johansson, M. Almqvist, J. Nilsson and T. Laurell, *Sens. Actuators, B*, 2005, **106**, 851–858.
- 12 M. Saito, N. Kitamura and M. Terauchi, *J. Appl. Phys.*, 2002, **92**, 7581–7586.
- 13 A. Haake, A. Neild, G. Radziwill and J. Dual, *Biotechnol. Bioeng.*, 2005, **92**, 8–14.
- 14 A. Neild, S. Oberti, G. Radziwill and J. Dual, *Biotechnol. Bioeng.*, 2007, **97**, 1335–1339.
- 15 S. Oberti, A. Neild and J. Dual, *J. Acoust. Soc. Am.*, 2007, **121**, 778–785.
- 16 S. M. Hagsater, T. G. Jensen, H. Bruus and J. P. Kutter, *Lab Chip*, 2007, **7**, 1336–1344.
- 17 J. J. Shi, D. Ahmed, X. Mao, S. C. S. Lin, A. Lawit and T. J. Huang, *Lab Chip*, 2009, **9**, 2890–2895.
- 18 O. Manneberg, B. Vanherberghen, J. Svennebring, H. M. Hertz, B. Önfelt and M. Wiklund, *Appl. Phys. Lett.*, 2008, **93**, 063901.
- 19 O. Manneberg, B. Vanherberghen, B. Önfelt and M. Wiklund, *Lab Chip*, 2009, **9**, 833–837.
- 20 J. Hultstrom, O. Manneberg, K. Dopf, H. M. Hertz, H. Brismar and M. Wiklund, *Ultrasound Med. Biol.*, 2007, **33**, 145–151.
- 21 O. Manneberg, J. Svennebring, H. M. Hertz and M. Wiklund, *J. Micromech. Microeng.*, 2008, **18**, 095025.
- 22 O. Manneberg, PhD thesis, Royal Institute of Technology, Stockholm, 2009.
- 23 R. Barnkob, P. Augustsson, T. Laurell and H. Bruus, *Lab Chip*, 2010, **10**, 563–570.
- 24 J. F. Spengler and W. T. Coakley, *Langmuir*, 2003, **19**, 3635–3642.
- 25 P. Glynne-Jones, R. J. Boltryk, N. R. Harris, A. W. J. Cranny and M. Hill, *Ultrasonics*, 2010, **50**, 68–75.
- 26 J. Svennebring, O. Manneberg and M. Wiklund, *J. Micromech. Microeng.*, 2007, **17**, 2469–2474.